Preclinical Modeling of Chronic Inhibition of the Parkinson's Disease Associated Kinase LRRK2 Reveals Altered Function of the Endolysosomal System in Vivo

JILLIAN H. KLUSS
National Institutes of Health
Melissa Conti Mazza
National Institutes of Health
Yan Li
National Institutes of Health
Claudia Manzoni
University College London
Patrick A. Lewis
RVC: The Royal Veterinary College
Mark R. Cookson (cookson@mail.nih.gov)
National Institute on Aging https://orcid.org/0000-0002-1058-3831
Adamantios Mamais
University of Florida McKnight Brain Institute

Research article

Keywords: Parkinson's Disease, LRRK2 chronic inhibition, proteomics, phospho-proteomics

Posted Date: September 25th, 2020

DOI: https://doi.org/10.21203/rs.3.rs-78203/v1

Version of Record: A version of this preprint was published on March 19th, 2021. See the published version at https://doi.org/10.1186/s13024-021-00441-8.

Abstract

Background

The most common mutation in the *Leucine-rich repeat kinase 2* gene (LRRK2), G2019S, causes familial Parkinson's Disease (PD) and renders the encoded protein kinase hyperactive. To date, the molecular effects of chronic LRRK2 inhibition have not yet been examined *in vivo*.

Methods

We evaluated the utility of newly available phospho-antibodies for Rab substrates pT73 Rab10, pS106 Rab12, pT71 Rab29 and LRRK2 autophosphorylation to examine the pharmacodynamic response to acute treatment paradigms with the potent and specific LRRK2 inhibitor, MLi-2, in brain and peripheral tissue in G2019S LRRK2 knock-in mice to define the relative target engagement between brain and LRRK2-enriched peripheral tissues. The molecular effects of 10 days and 10 weeks of chronic in-diet dosing were also evaluated using TMTpro reagents for LC-MS/MS total and phospho- proteomics in brain and kidney tissues.

Results

We report higher sensitivity of LRRK2 autophosphorylation to MLi-2 treatment and slower recovery in washout conditions compared to Rab GTPases phosphorylation, and we identify pS106 Rab12 as a robust readout of downstream LRRK2 activity across tissues. The downstream effects of long-term chronic LRRK2 inhibition *in vivo* were evaluated in G2019S LRRK2 knock-in mice by phospho- and total proteomic analyses following an in-diet administration of MLi-2 for 10 weeks. We observed alterations in endolysosomal and trafficking pathways in the kidney that were sensitive to MLi-2 treatment and that we validated biochemically. Furthermore, a subtle but distinct biochemical signature affecting mitochondrial proteins was observed in brain tissue in the same animals that was reverted by kinase inhibition.

Conclusions

This is the first study to examine the molecular underpinnings of chronic LRRK2 inhibition in a preclinical *in vivo* PD model and highlights cellular processes that may be influenced by therapeutic strategies aimed at restoring LRRK2 physiological activity in PD patients.

Background

Mutations in *leucine-rich repeat kinase 2* (*LRRK2*) are a known genetic cause of familial Parkinson's disease (PD) (1–3). Non-coding variation at the *LRRK2* locus has also been identified as a risk factor for sporadic PD, suggesting that both disease forms share common pathological mechanisms (4,5). The G2019S mutation, which lies within the kinase domain of LRRK2, is the most common mutation found in familial PD cases, as well as in 1-5% of sporadic PD patients (6). This mutation directly increases kinase activity while other mutations likely have convergent cellular effects, albeit through varying mechanisms

(4). Therefore, it is thought that targeting LRRK2 therapeutically may be advantageous in both familial and sporadic PD (7,8).

A number of pharmacological tools that inhibit LRRK2 kinase activity in the CNS have been developed and characterized (9). Some kinase inhibitors have been shown to reduce cytotoxicity associated with LRRK2 mutations in PD-relevant cell and animal models (10–12), supporting the hypothesis that LRRK2 inhibition may be efficacious for PD. One such LRRK2-specific inhibitor, MLi-2, has been found to be ~300x more selective for LRRK2 over other kinases and can readily cross the blood-brain barrier (13) demonstrating that it is possible to generate tool compounds that have clinical potential for therapeutic intervention in PD. However, as LRRK2 is expressed endogenously in many tissues and kinase inhibition is predicted to affect both mutant and wild-type LRRK2, whether such inhibitors would be safe to use clinically is uncertain. Preclinical studies have reported macroscopic changes *in vivo* that include morphological changes in lung from nonhuman primates, and kidney tissue from rats treated with specific LRRK2 inhibitors that are reversible after termination of treatment (14–16). Importantly, some of these effects overlap with those seen in Lrrk2 knockout mice (17) demonstrating that they result from on-target effects of inhibitors on LRRK2 itself rather than resulting from inhibition of other kinases.

Here, we aimed to mimic a likely clinical use of LRRK2 inhibitor to understand the relationship between level of inhibition and effects on biochemistry of target tissues including brain and peripheral organs that express high levels of LRRK2. We first evaluated the utility of measuring autophosphorylation of LRRK2 versus downstream substrate Rab proteins as readouts of LRRK2 kinase activity *in vivo* across a series of acute and chronic dosing paradigms in kinase hyperactive G2019S LRRK2 knock-in mouse model. Secondly, we explore the molecular effects of long-term chronic LRRK2 inhibition by unbiased total and phospho-proteomics on brain and kidney tissue from G2019S LRRK2 mice following 60mg/kg/day in-diet dosing of MLi-2 for 10 weeks. Based on these data, we report molecular pathways that are affected by chronic inhibition of LRRK2 in a clinically relevant paradigm. Importantly, we show that the effects of LRRK2 inhibition vary across tissues, which may be particularly relevant to selection of biomarkers for clinical trials where brain target engagement is inferred from peripheral tissue events.

Methods

Animals

All animal procedures were performed in accordance with a protocol approved by the Institutional Animal Care and Use Committee of the National Institute on Aging, NIH. Wildtype, G2019S LRRK2 knock-in (KI), and LRRK2 knockout (KO) male and female mice raised on a C57Bl/6 background (3-8 months in age) were bred in-house on a 12-hour day/night cycle for the following experiments. All mice were supplied with Rodent NIH-07 diet and water *ad libitum*.

Acute MLi-2 dosing

Dose response: Twenty-eight homozygous G2019S KI C57BL/6J mice (5–8 months old) were randomized for treatment using the sample function in R, followed by matching for sex across groups. Mice were given an acute dose of vehicle [40% (w/v) Hydroxypropyl-β-Cyclodextran] or MLi-2 (at 1, 3, 10, 30, 60, or 90 mg/kg dissolved in vehicle) via oral gavage and euthanized 1 hr after treatment. Based on our previous data on S1292 dephosphorylation in G2019S LRRK2 brain following acute MLi-2 treatment (18), N=4 was used in this study for all acute MLi-2 experiments, as it was estimated at 90% power to detect a difference of effect size 6 at alpha=0.05.

Time course: Twenty-eight homozygous G2019S KI C57BL/6J mice (4–7 months old) were randomized for treatment using the sample function in R, followed by matching for sex across groups. Mice were given an acute dose of vehicle [40% (w/v) Hydroxypropyl-β-Cyclodextran] at time point zero, or MLi-2 (10mg/kg dissolved in vehicle) via oral gavage and euthanized after time point 0.5, 1, 3, 12, 24, or 72 hrs post dose.

Chronic in-diet dosing

To determine the appropriate concentration of MLi-2 necessary to achieve S1292 phosphorylation levels that are comparable to the brain tissue levels in a wildtype animal, homozygous G2019S KI mice were given customized Rodent NIH-07 chow from Research Diets, either untreated or supplemented with various doses of MLi-2 (10, 30, or 60mg/kg/day) for ten days along with an untreated wildtype group, and S1292 phosphorylation signal was measured via Western blot (N=3 mice were used per treatment group). Mice and chow were weighed daily to assess estimated doses of MLi-2 received each day. No difference was observed in food intake between mice receiving MLi-2 treated chow and mice receiving untreated chow. All mice were given chow and water *ad libitum*. After ten days, mice were euthanized 2-3hrs post start of their light cycle.

10 day (short-term) and 10 week (long-term) chronic cohorts: Three-month old littermates from wildtype, homozygous G2019S KI, and homozygous LRRK2 KO mice were randomized into short-term (10 days) and long-term (10 weeks) chronic treatment groups: wildtype, G2019S KI, and LRRK2 KO groups received untreated chow, and a G2019S KI group received chow supplemented with 60mg/kg of MLi-2 per day. Both male and female mice were represented equally in all treatment groups (N=6 mice were used per treatment group). All mice were given chow and water *ad libitum*. After 10 days, or 10 weeks, mice were euthanized 2-3hrs post start of their light cycle.

Statistical Analyses

Statistical analyses for each experiment can be found within each respective figure legend. Briefly, one-way ANOVA or two-way ANOVA with Tukey's post hoc-test were used which were performed in GraphPad Prism v8.2.0 (GraphPad Software, San Diego, CA). If not otherwise stated, comparisons were considered statistically significant where $p < 0.05$. *, $p < 0.05$; **, $p < 0.01$; ***, $p < 0.001$; ****, $p < 0.0001$.

Immunoblotting

Tissues were homogenized at 20% w/v in 1x Cell Signaling Lysis Buffer (#9803S) with 1x protease and phosphatase inhibitors (Thermofisher; #1861279 and #78427, respectively) and left on ice for 30 minutes to lyse. Homogenates were spun at 20,000g for 10 minutes at 4 degrees Celsius and pelleted debris were removed. Samples were supplemented with NuPage LDS sample buffer 4x (#NP0008), boiled for 5 min at 95 degrees Celsius and run on a Bio-Rad Criterion™ TGX™ polyacrylamide gel (#5671095) at 200 V for 37 min. Gels were transferred to nitrocellulose (#1704159) on a Bio-Rad Trans-Blot. Turbo™ transfer system at 20 V for 10 min. The nitrocellulose was blocked for 1 h in 50% TBS (20 mM Tris, 0.5 M NaCl, pH 7.5), 50% Odyssey blocking buffer (Li-Cor; 927–40,000) and incubated overnight with primary antibodies in 50% TBS-T (20 mM Tris, 0.5 M NaCl, pH 7.5, 0.1% Tween 20), 50% Odyssey blocking buffer at 4 degrees Celsius. Following 3 x 5 min washes with TBS-T, the nitrocellulose was incubated at RT with secondary antibodies for 1 hr, washed 3 x 5 min and scanned at the Li-Cor platform.

All primary antibodies and working dilutions can be found in Additional file 1. Secondary antibodies were used at 1:10,000 dilution: IRDye. 800CW Goat anti-Rabbit IgG (LiCor: 926–32211), IRDye. 680RD Goat anti-Mouse IgG (LiCor: 926-68070). All blots presented in each figure panel were derived from the same experiment and were processed in parallel. Raw densitometric signal was normalized to a common normalizer sample that was run on every blot.

Tissue preparation for proteomics and phosphoproteomics

One brain hemisphere and one half of a kidney from each mouse in the short-term and long-term chronic experiments were processed and submitted for proteomics and phosphoproteomics analysis using TMT quantitation without and with TiO_2/iMAC enrichment. Briefly, tissues were homogenized in 15% w/v lysis buffer (0.5mM HEPES, pH7.4, 225mM mannitol, 50mM sucrose, 1mM EDTA, 1x protease and phosphatase inhibitors (Thermofisher; #1861279 and #78427, respectively), and 2% CHAPS) followed by incubation on ice for 30 min, with periodic vortexing, to lyse. The homogenates were then spun down at 20,000g at 4 degrees Celsius for 10 min to pellet cellular debris. A protein assay was performed on supernatants to determine protein concentration, and 270µg of each sample were submitted for mass spectrometry. Additionally, 30µg of each sample were pooled together to allow for normalization between runs during analysis.

Phosphoproteomics and Bioinformatics Analysis

Proteins were alkylated with NEM, digested with trypsin and labeled with TMTpro reagents. The brain and kidney samples were treated with the same method. 48 brain/kidney samples and 4 pooled samples were separated into 4 sets of TMT experiments. Each set contains 12 samples and one pooled sample. The pooled sample in each set was labeled with TMTpro-126 reagent, while the distribution and labeling of 12 samples were randomized. After the labeling and quenching, samples were combined together. 95% of the combined sample was used for phosphopeptide enrichment using TiO2 method followed by iMAC method. 5% of the combined sample was fractionated using Pierce high pH reverse phase cartridge, and 8 fractions were collected for each set. LC-MS/MS data acquisition were performed on a Thermo

Scientific Orbitrap Lumos mass spectrometer which was coupled to a Thermo Scientific Ultimate 3000 HPLC. Peptides were separated on an ES802 nano-column over 136 minutes at a flow rate of 300 n/min. TMT MS2 method was used. Both MS1 and MS2 scans were performed in orbitrap. The resolution for MS1 and MS2 scans were 120K and 50K, respectively. Peptides were fragmented using the HCD method with collision energy fixed at 32%. The precursor isolation window is 1.5 Da.

Proteome Discoverer 2.4 was used for database search and TMT quantitation. Ratios of raw abundance values of each sample over the pooled sample were generated and analyzed in R using the limma package (version 4.0, empirical Bayes method) (19). Briefly, the proteomics datasets from four MS runs were combined and only hits that were detected in at least 4 out of 6 mice were kept, while the missing 1-2 values were imputed. These phospho-peptide and total protein datasets were merged and matched for accession number and the ratio of phospho/total abundance was generated. Principal component analysis was conducted for these datasets which revealed a modest batch effect that was corrected computationally. Statistical analyses were conducted, namely t-tests between pairs were visualized as volcano plots (20), and z scores were calculated for heatmaps. Proteins were considered significant hits with an adjusted p-value <0.05, and for kidneys a fold change >1.4. Functional enrichment analysis of the significant hits was performed using the R package gProfiler2 (precision cutoffs of adjusted p-values were <1e-6 and ,<1e-20 for kidney and brain hits, respectively) (21). Enrichment term networks were visualized using Cytoscape 3.7 (22).

Human LRRK2 interactome analyses

We generated a human interactome of LRRK2 and compared it with the significant hits found in kidney total and phospho- proteomics using the PINOT searching tool (http://www.reading.ac.uk/bioinf/PINOT/PINOT_form.html) which collates published, experimentally validated protein-protein interaction (PPI) data from 7 different databases (bhf-ucl, BioGRID, InnateDB, IntAct, MBInfo, MINT and UniProt), merged the annotations and performed quality control providing a final score indicative of reproducibility (23). The PPIs of LRRK2 with a final score >2 were kept as first layer interactors (i.e. reported in literature as able to directly bind to LRRK2). The first layer interactors of LRRK2 (220 proteins) were used as input in PINOT to download PPIs able to bind directly to the first layer (i.e. second layer interactors). The second layer interactors are proteins that are able to connect to LRRK2 via their direct connection with a protein within the first layer (Data file S1). Scripts were run in R (3.6.2) and networks were drawn using Cytoscape 3.5, mouse to human protein ID conversion was performed using g:Profiler (21).

Results

Relative sensitivity of LRRK2 autophosphorylation and Rab GTPase phosphorylation to MLi-2 inhibition in vivo

Our aim in this series of studies was to mimic a likely clinical scenario where mutant LRRK2 is inhibited to levels similar to that seen with wild type protein, thus nullifying the potential toxic effects of enhanced

pathogenic kinase activity. In order to be able to model this situation, we first needed to identify reliable markers of LRRK2 activity *in vivo* and understand the relationship between peripheral organ and brain target engagement. To this end, we compared the response of phosphorylation of LRRK2 itself and downstream Rab substrates to MLi-2 *in vivo* using two acute treatment paradigms.

First, we investigated the dose responsiveness of LRRK2 autophosphorylation and phosphorylation of Rab GTPases to acute kinase inhibition *in vivo*. G2019S KI mice were given an acute dose of MLi-2 at 1, 3, 10, 30, 60, or 90mg/kg or vehicle via oral gavage and sacrificed 1hr post dose. We observed significant pS1292 dephosphorylation starting at the lowest dose of 1mg/kg in kidney and lung (Fig. 1A, B). Maximal dephosphorylation was achieved in the brain, kidney and lung at 10mg/kg for both pS1292 and pS935 (Fig. 1A - C). Maximal S1292 dephosphorylation in the brain did not exceed 60% signal decrease with increasing MLi-2 concentrations, suggesting that maximal inhibition was achieved. The S935 phospho-site had lower IC50 compared to pS1292 in the brain, suggesting that this marker is more sensitive to LRRK2 inhibition *in vivo*

Phosphorylated Rab GTPases showed more variable responses to MLi-2 across tissues. The T73 Rab10 phospho-site responded significantly to MLi-2 treatment in peripheral tissues but not in the brain (Fig. 1A, D). Phospho- S106 Rab12 showed a robust response to MLi-2 in both brain and peripheral tissues with maximal dephosphorylation at 30-60mg/kg (Fig. 1A, E; antibody validation experiments are shown in Supplementary figs. 1 and 2). The T71 Rab29 phospho-site responded with treatment in all tissues but with higher variability compared to Rab12, especially at lower doses (Fig. 1A, F). At 10mg/kg, we saw ~50% decrease in Rab10, Rab12 and Rab29 phosphorylation in the periphery while higher doses retained ~30% residual phosphorylation signal. These results demonstrate that 10mg/kg of MLi-2 is adequate to acutely inhibit LRRK2 autophosphorylation in brain and peripheral tissues. Based on these results, we selected a dose of 10mg/kg MLi-2 for subsequent time course analyses and washout experiments.

Time course of acute MLi-2 administration reveals that phosphorylation of Rab GTPases recovers faster than LRRK2 phosphorylation

To further discriminate how LRRK2 and Rab phosphorylation events vary between brain and peripheral tissues, we compared time courses and recovery after washout of inhibitor application. An acute dose of MLi-2 at 10mg/kg was administered via oral gavage to G2019S KI mice and sacrificed at 0.5, 1, 3, 12, 24, or 72 hours post dose. A time point of 0 hours was included where animals were given an equivalent dose of vehicle and euthanized immediately thereafter to measure baseline phosphorylation.

Phospho- S1292 and S935 LRRK2 showed rapid dephosphorylation at 0.5hrs, with maximal dephosphorylation achieved at 1hr post dose across all tissues (Fig. 2A - C). The dephosphorylation patterns of both phospho-sites tightly correlated between brain, kidney, and lung tissues. Interestingly, maximal dephosphorylation for all pRabs was seen at 1hr in all tissues. However, these sites recovered more rapidly than pLRRK2 (~12hrs versus 24hrs; Fig. 2A, D - F). Measures of T73 Rab10 signal in brain tissue did not show MLi-2-dependent dephosphorylation compared to peripheral tissues (Fig. 2A, D). Dephosphorylation of T71 Rab29 was achieved in all three tissues to varying degrees, with kidneys

showing the strongest response to MLi-2, reaching ~75% dephosphorylation compared to 20-30% seen in brain and lung tissue (Fig. 2A, F). pS106 Rab12 mimicked pLRRK2 most closely in that all tissues showed similar dephosphorylation patterns over time and reached a maximum of 60% dephosphorylation (Fig. 2A, E). It was also noted that Rab12 phosphorylation showed the least variability across mice compared to Rab10 and Rab29. These data suggest that Rab GTPases are dephosphorylated within the first hour after LRRK2 inhibition in a similar fashion to LRRK2 dephosphorylation, with Rab12 performing similarly to pLRRK2 in the brain and periphery. In contrast, the kinetics of Rab GTPase re-phosphorylation show a quicker recovery (~12hrs) compared to LRRK2 (~24hrs).

In-diet MLi-2 administration can diminish G2019S-dependent hyperphosphorylation to wild type levels

To evaluate the molecular effects of chronic LRRK2 inhibition, we first conducted a dose response experiment of MLi-2 in diet. With clinical relevance in mind, our aim was not to fully inactivate LRRK2, as inferred from a complete dephosphorylation of S1292, but to ameliorate the hyperphosphorylation to a range observed in wildtype animals.

G2019S KI mice were fed a customized rodent chow supplemented with MLi-2 to achieve 10, 30, or 60 mg/kg/day dosing. For reference, we included wildtype and G2019S KI mice that were fed control chow for 10 days. In the treated animals, we observed that 60mg/kg/day diminished S1292 phosphorylation to wildtype levels in brain and kidney, whereas a 10mg/kg/day dose was sufficient to decrease phosphorylation to wildtype levels in lung tissue (Fig. 3A, B). This suggests some peripheral tissues with enrichment of LRRK2 may be more sensitive to drug-induced inhibition. Increasing doses of MLi-2 show a dose response in pS935 LRRK2 (Fig. 3A, C). These results confirm a dose of 60mg/kg/day is sufficient to inhibit G2019S LRRK2 to wild type levels in vivo across tissues.

Chronic MLi-2 treatment in G2019S KI mice results in sustained LRRK2 and Rab12 dephosphorylation

To extend these results into a chronic timescale, G2019S KI mice were given customized chow supplemented with MLi-2 to reach a 60 mg/kg/day dose for 10 days or 10 weeks. Control groups of wildtype, G2019S KI, and LRRK2 KO mice receiving untreated chow were included for reference of baseline phosphorylation patterns. For the purpose of this experiment, we refer to the 10-day cohort as ‘short-term’ and the 10-week cohort as ‘long-term’ treatment groups. The schematic in Fig. 4A depicts the design of this experiment, in which brain, kidney, and lung tissues were collected and processed for Western blot analyses, and the 10-week cohort tissues were additionally prepped for total and phospho-proteomics. Body weight and estimated food intake for each mouse was recorded daily to determine the daily dose of MLi-2 each mouse received (Fig. 4B - G). Both short- and long-term cohorts received the appropriate dose of MLi-2 and had comparable chow intake of ~4g, while weight increase was observed only in the 10-week cohort, particularly in the LRRK2 KO animals.

In both short-term and long-term cohorts, pS1292 levels of G2019S KI mice treated with MLi-2 were significantly decreased to levels comparable to wildtype mice (Fig. 5A - C). In the long-term cohort, mice treated with MLi-2 showed further dephosphorylation compared to wildtype levels in lung (Fig. 5C). S106

Rab12 showed significant dephosphorylation consistent throughout tissues, similar to the response of LRRK2 dephosphorylation (Fig. 5A, H - I), proving pRab12 is a reliable readout of LRRK2 activity and inhibition in this model. Additionally, phosphorylation of S935 LRRK2 was significantly reduced in all tissues compared to both G2019S and wildtype untreated animals in both cohorts as expected (Fig. 5A, D - E). In contrast, and similar to the tissue and dose-specific responses to acute inhibition, Rab10 and Rab29 did not respond consistently to LRRK2 inhibition in this chronic paradigm (Supplementary fig. 3). Furthermore, total LRRK2 levels in the short-term cohort were significantly decreased in MLi-2-treated mice compared to their untreated counterparts in kidney and lung tissues, which was exacerbated in the long-term treatment across all tissues (Fig. 5A, F - G). This suggests chronic inactivation of LRRK2 leads to protein degradation, consistent with previous in vivo and in vitro studies using MLi-2 and other LRRK2 inhibitors (13,24).

Unbiased proteomics reveal both therapeutic and dysregulatory effects in endolysosomal, trafficking, and mitochondrial pathways with chronic LRRK2 inhibition in mice

The above studies identified a chronic dosing regimen in which amelioration of the hyperphosphorylation of the S1292 autophosphorylation LRRK2 site and pS106 Rab12 in G2019S KI mice can be achieved to levels seen with wildtype LRRK2 at the endogenous level in vivo. We next used a series of proteomics approaches to determine, in an unbiased manner, what the consequences of this treatment might be to tissue proteome.

Proteomic analysis revealed 115 total proteins and 34 phospho-proteins that were differentially expressed in the kidney between chronic MLi-2-treated and untreated G2019S LRRK2 mice (false-discovery rate (FDR) adjusted $p < 0.05$; fold change (FC) > 1.4); (Fig. 6A, B). Among the top differentially abundant proteins, there was a strong enrichment for endolysosomal, trafficking and mitochondrial proteins (Fig. 6A, C). Multiple lysosomal proteins showed differential abundance, including cathepsin B (Ctsb), legumain (Lgmn), galactosidase beta 1 (Glb1), Lysosomal-associated membrane protein 1 (Lamp1), and N-acetylglucosamine-6-sulfatase (Gns). In addition, a number of proteins involved in vesicular trafficking, lipid metabolism, iron uptake and mitochondrial function were also significantly altered in kidneys of chronically treated animals. Hierarchical clustering of differential proteins in the G2019S MLi-2 treated group showed most similarity to the LRRK2 KO animals (Fig. 6C), suggesting that chronic inhibition of LRRK2 may mimic features of an absence of LRRK2 in the periphery. Among the significant phosphoprotein hits, additional trafficking and mitochondrial proteins were identified, including sorting nexin 1 (pS188 Snx1) and vacuolar sorting protein 4b (pS102 Vps4b) (Fig. 6D). Analysis using Gene Ontology databases of significant hits from total and phospho-proteins showed enrichment of the endolysosomal system as well as mitochondrial membrane (Fig. 6E).

Additionally, we analyzed the human homologs of total and phospho-protein hits *in silico* to identify a LRRK2 protein-protein interactome using PINOT (*19*). We converted the 115 total proteins and 34 phospho-proteins that were differentially expressed in the kidney between chronic MLi-2-treated and untreated G2019S LRRK2 mice to their human orthologues and identified 76 matches within the LRRK2

interactome. Five of the matching proteins (AHCYL1, EEF2, HSP90AA1, HSP90AB1 and RANBP2) were present in the first layer while 71 in the second layer of LRRK2 interactions. The difference between the average random result from 100,000 simulated experiments (40 matches) and the real result (76 matches) was highly significant ($p=2.78*10^{-11}$). The matching proteins were extracted from the LRRK2 interactome and their connectivity with LRRK2 visualized (Supplementary fig. 4). This high degree of connectivity suggests that these proteins are in fact related to LRRK2 biology rather than an effect of MLi-2 treatment itself.

Proteomic analysis of brain tissue of 10-week MLi-2-treated mice revealed a number of mitochondrial proteins that showed statistically significant p-value (adjusted $p<0.05$) compared to untreated G2019S KI controls, albeit with modest fold differences between treatment groups (Fig. 7A, B). These include Cytochrome C, NADH:Ubiquinone Oxidoreductase Subunit V3 (Nduvf3), the mitochondrial ATP synthase Atp5g1 and Voltage Dependent Anion Channel 2 (Vdac2) (Fig. 7A, B). Phospho-proteomics analysis revealed a decrease in S58 phosphorylation of the ion transporter Fxyd7 and increase in S109 phosphorylation of the PP2A inhibitor Ensa (Fig. 7B). Cumulative Gene Ontology analysis revealed enrichment for proteins residing in different mitochondrial compartments as well synaptic proteins (Figure 7C). These data suggest that even though the brain is more resilient in terms of potential endolysosomal defects that may be associated with LRRK2 inhibition, there are small changes in mitochondrial function resulting from chronic LRRK2 inhibition. Volcano plots comparing untreated groups of G2019S KI and wildtype mice showed that a number of proteins had the opposite trend to that seen in the chronic MLi-2 cohort (Fig. S5). For example, the transmembrane ion transporters Sfxn2 and Sfxn3, showed a modest upregulation in kidneys of G2019S LRRK2 compared to wildtype mice and this was rescued in the chronic MLi-2 G2019S LRRK2 cohort (Figs. 6A and Supplementary fig. 5A). For some mitochondrial proteins identified in our brain proteomics screen, Cytochrome C, Vdac1, Ndufs3, and Ndufv2 were downregulated in G2019S LRRK2 brain compared to wildtype and this was reversed in the chronic MLi-2 G2019S LRRK2 cohort (Figs. 7A and Supplementary fig. 5B). This suggests that treatment can significantly alter the expression of mitochondrial proteins in G2019S KI mice in a direction consistent with therapeutic potential.

Validation of endolysosomal, trafficking, and mitochondrial proteins in chronically LRRK2 inhibited mice reveal both a rescue of mutant-driven effects and dysregulatory patterns in vivo

We next wanted to validate protein hits observed from our proteomics screens in kidney tissue. Through Western blot analyses, we found two distinct patterns of effects, one we characterized as beneficial, based on a reverse in protein expression from G2019S KI animal levels back to wildtype levels and the other dysregulatory, based on a mimicking effect comparable to LRRK2 KO animals (Fig. 8A). In the former category, the non-glycosylated form of Lamp1, the ESCRT-0 protein Hgs, and the iron and serine mitochondrial transporter Sfxn3 were all shown to be significantly increased in protein levels in untreated G2019S KI mice compared to wildtype animals. These levels were ameliorated back to wildtype levels after MLi-2 treatment for 10 weeks (Fig. 8B). Conversely, the glycosylated form of Lamp1 and the lysosomal hydrolase Legumain were both significantly increased in the same animals, patterns of which

have been previously characterized in LRRK2 KO animals, and is recapitulated here in our LRRK2 KO mice in this cohort (25). In addition, we also discovered that the motor adaptor protein Jip4 was significantly reduced in LRRK2 KO mice, and this was also seen in G2019S KI mice treated with MLi-2 (Fig. 8C). Interestingly, this phenotype is kidney-specific, as no significant difference of these proteins was observed in brain or lung tissues (not shown). Additionally, these differences were not seen in mice that were treated with MLi-2 for only 10 days (Supplementary fig. 6), suggesting that chronic inhibition of LRRK2 is necessary to see these effects.

Discussion

In the present study, we have evaluated various markers of LRRK2 inhibition *in vivo* and demonstrated their utility across brain and peripheral tissues. In both acute and chronic treatment paradigms, we focused on a treatment paradigm that might reasonably mimic clinical applications where the hyperactive mutant of LRRK2, G2019S, expressed at the endogenous level is chronically depressed to that of wild type animals. We performed proteomics to examine the molecular effects of chronic LRRK2 inhibition and identified changes to the endolysosomal, trafficking, and mitochondrial systems in kidneys at the total protein level as well as phosphorylation events. In addition, we noted a modest but statistically significant change in mitochondrial proteins, most notably enriched within the mitochondrial electron transport chain, in the brains of MLi-2 treated G2019S mice.

In our studies in mouse tissue, measuring LRRK2 phosphorylation, particularly the pS1292 autophosphorylation site, provides the most reliable marker of both G2019S-induced hyperactivity and MLi-2 dependent inhibition. Whether this can be extrapolated to human clinical samples is unclear as current tools have not yet allowed for robust detection of pS1292 LRRK2 in peripheral blood, although some studies have demonstrated its efficacy in urinary and CSF exosomes (26,27). Using the commercially available pRab antibodies, we found that S106 Rab12 phosphorylation pattern resembled that of pS1292 LRRK2 most closely across experiments, in that G2019S KI mice displayed hyperphosphorylation that was ameliorated with MLi-2 treatment. This is in contrast to the hyperphosphorylation pattern of other Rab substrates, which have been demonstrated in mutations within the GTPase domain but not for G2019S (28,29). Thus, for G2019S-carriers and potentially other PD cases, detection of pRab12 has potential as a biomarker for LRRK2 activity and inhibition.

Using these two validated biomarkers of pS1292 LRRK2 and pS106-Rab12, a 60mg/kg/day dosing of MLi-2 in G2019S KI mice via in-diet dosing for 10 days or 10 weeks was shown to be sufficient to revert the hyperactive mutation approximately to wild type levels. Such an approach could be helpful in identifying similar dosing regimens in humans. Importantly, we show that measurements in some peripheral tissues, particularly kidney, reflect events in the brain, the likely target organ for any PD clinical trial. However, we observed that after long-term chronic MLi-2 in-diet dosing, S1292 LRRK2 and S106 Rab12 phosphorylation was significantly lower than wildtype levels in lung. It is possible that lung tissue is more sensitive to LRRK2 inhibition than other tissues considered here and has also been suggested in a recent study investigating the toxicological and morphological effects of LRRK2 inhibition on

nonhuman primate lungs, in which high doses of three structurally distinct LRRK2-specific inhibitors, including MLi-2, induced vacuolated cytoplasm in type II pneumocytes, however no pulmonary deficits were observed (16). These data suggest that there is a lung-specific LRRK2-dependent mechanism that is affected by chronic LRRK2 inhibition. Total LRRK2 levels showed a decrease in kidney in the chronic treatment cohort compared to untreated G2019S KI mice suggesting that LRRK2 is targeted for degradation following kinase inhibition (24). Overall, these data suggest that while LRRK2 inhibitors can be used to diminish hyperactive kinase to wild type levels of activity, there are tissue-specific differences in activity and stability of the protein that may be important to consider when using peripheral engagement to infer brain inhibition.

Unbiased proteomic screens revealed significant differences in endolysosomal, trafficking, and mitochondrial proteins in the kidneys of treated compared to untreated G2019S KI animals. We identified two subsets of proteins, those that suggest a therapeutic effect and those that are dysregulatory, with long-term chronic LRRK2 inhibition *in vivo*. Strikingly, all differential changes were specific to our 10-week treatment cohort compared to our 10-day cohort. This suggests that these molecular changes are specific to the length of LRRK2 inhibition. Thus, future preclinical efforts are needed that include long-term inhibitor treatment in order to understand what may happen in human disease. Proteins altered towards a therapeutic effect included non-glycosylated Lamp1, Hgs, and Sfxn3, whereas glycosylated Lamp1, leguman, and Jip4 showed likeness to LRRK2 KO expression levels. Based off of these proteins, we hypothesize a mechanism for the endolysosomal trafficking pathway in the context of both LRRK2 kinase hyperactivity and chronic inhibition, in which both dysfunctional LRRK2 kinase states converge on the same pathway through different means depicted in Fig. 8D.

In brain tissue, chronic MLi-2 treatment in G2019S KI mice showed a modest but significant upregulation of mitochondrial proteins compared to their untreated counterparts. Production of reactive oxygen species (ROS), mitochondrial elongation, decreased ATP production and mitochondrial DNA damage have been reported in G2019S PD patient-derived skin biopsies and G2019S-LRRK2 *in vitro* models (30–34). In brain tissue, the majority of mitochondrial proteins found in our screens were associated with the respiratory chain Complex I and III. Further studies are needed in order to elucidate the effects of LRRK2 on the respiratory chain system. However, these results do not suggest a potential concern for LRRK2 kinase inhibition affecting mitochondrial function as in general they respond in the opposite direction of effect to the pathogenic G2019S mutation, i.e. are in the therapeutic direction. A limitation of this study is that whole brain homogenate was used for the proteomics analysis which may have limited our ability to determine regional- and cell type-dependent LRRK2 mechanisms. Further studies focused on regional and cell-specific parameters can shed a deeper mechanistic insight into the molecular consequences of LRRK2 inhibition in the brain.

Conclusion

The aim of the present study was twofold: to assess the suitability of new antibodies of known LRRK2 substrates as biomarkers for LRRK2 kinase inhibition and to evaluate what molecular effects are

observed when LRRK2 is chronically inhibited. We found that pRab12 is a reliable readout of LRRK2 activity and inhibition, and that phosphorylation patterns seen in the periphery reflect events in the brain. Additionally, our study highlights the molecular effects of chronic inhibition that remain to be explored and warrant further investigation in the light of the ongoing clinical trials. What remains to be determined is which of these effects are truly protective or damaging, and how relevant they are to what happens in human disease.

As of yet, there continues to be a significant unmet medical need in the field of neurodegeneration for effective, long lasting treatments that either halt or slow disease progression. Existing drug treatments for PD target the symptoms of the disease rather than cause, and do not modify disease course. Clinical trials are currently underway to assess the safety and efficacy of LRRK2-specific kinase inhibition in PD patients (35). In parallel with these trials, future work will need to elucidate the underlying disease mechanisms that cause PD and how LRRK2 mutations ultimately lead to neurodegeneration. Understanding the pathobiological role of LRRK2 kinase activity will greatly aid in the development and optimization of therapeutic strategies.

Abbreviations

Ctsb: Cathepsin B

Glb1: β-galactosidase

Glut4: Glucose transporter 4

Gns: N-acetylglucosamine-6-sulfatase

Hgs: Hepatocyte growth factor-regulated tyrosine kinase substrate

Jip4: JNK-interacting protein 4

Lamp1: Lysosomal-associated membrane protein 1

Lgmn: Legumain (or AEP, asparaginyl endopeptidase)

LRRK2: Leucine-rich repeat kinase 2

MLi-2: Merch LRRK2 inhibitor 2

Ndufa2: NADH dehydrogenase [ubiquinone] 1 alpha subcomplex subunit 2

Ndufs3: NADH dehydrogenase [ubiquinone] iron-sulfur protein 3

Ndufv3: NADH dehydrogenase [ubiquinone] flavoprotein 3

PD: Parkinson’s disease

ROS: Reactive oxygen species

Sfxn3: Sideroflexin 3

Snx: Sorting nexin 1

TGN: *Trans*-Golgi network

Vdac2: Voltage Dependent Anion Channel 2

Vps4b: vacuolar sorting protein 4b

Declarations

Availability of data and materials:

Raw LC-MS/MS data and supplementary files will be uploaded to ProteomeXchange.

Competing interests:

The authors declare that they have no competing interests.

Funding:

This study was supported in part by the Intramural Research Program of the NIH, National Institute on Aging, the Michael J. Fox Foundation for Parkinson's Research, the Medical Research Council, and the University of Reading.

Author contributions:

A.M., J.H.K. and M.R.C. conceptualized the project. M.C.M. performed all oral gavages for the acute treatment experiments. Y.L. performed TMT mass spectrometry experiments. C.M. performed the in-silico LRRK2 interactome analysis. J.H.K. performed all other experiments. J.H.K., P.A.L., M.R.C. and A.M. wrote the manuscript. All authors read and approved the final manuscript.

Acknowledgments:

We thank Dr. Heather L. Melrose, Mayo Clinic, for the gift of the G2019S LRRK2 mouse line. We thank Dr. Huaibin Cai, NIA, for the gift of the Lrrk2 KO mouse line.

References

1. Rudenko IN, Cookson MR. Heterogeneity of leucine-rich repeat kinase 2 mutations: genetics, mechanisms and therapeutic implications. Neurother J Am Soc Exp Neurother. 2014 Oct;11(4):738–50.

2. Greggio E, Jain S, Kingsbury A, Bandopadhyay R, Lewis P, Kaganovich A, et al. Kinase activity is required for the toxic effects of mutant LRRK2/dardarin. Neurobiol Dis. 2006 Aug 1;23(2):329–41.
3. West AB, Moore DJ, Choi C, Andrabi SA, Li X, Dikeman D, et al. Parkinson's disease-associated mutations in LRRK2 link enhanced GTP-binding and kinase activities to neuronal toxicity. Hum Mol Genet. 2007 Jan 15;16(2):223–32.
4. Cookson MR. The role of leucine-rich repeat kinase 2 (LRRK2) in Parkinson's disease. Nat Rev Neurosci. 2010 Dec;11(12):791–7.
5. Kluss JH, Mamais A, Cookson MR. LRRK2 links genetic and sporadic Parkinson's disease. Biochem Soc Trans. 2019 Mar 5;BST20180462.
6. Healy DG, Falchi M, O'Sullivan SS, Bonifati V, Durr A, Bressman S, et al. Phenotype, genotype, and worldwide genetic penetrance of LRRK2-associated Parkinson's disease: a case-control study. Lancet Neurol. 2008 Jul 1;7(7):583–90.
7. Alessi DR, Sammler E. LRRK2 kinase in Parkinson's disease. Science. 2018 Apr 6;360(6384):36–7.
8. West AB. Achieving neuroprotection with LRRK2 kinase inhibitors in Parkinson disease. Exp Neurol. 2017 Dec 1;298:236–45.
9. Estrada AA, Sweeney ZK. Chemical Biology of Leucine-Rich Repeat Kinase 2 (LRRK2) Inhibitors. J Med Chem. 2015 Sep 10;58(17):6733–46.
10. Eguchi T, Kuwahara T, Sakurai M, Komori T, Fujimoto T, Ito G, et al. LRRK2 and its substrate Rab GTPases are sequentially targeted onto stressed lysosomes and maintain their homeostasis. Proc Natl Acad Sci U S A. 2018 25;115(39):E9115–24.
11. Daher JPL, Abdelmotilib HA, Hu X, Volpicelli-Daley LA, Moehle MS, Faser KB, et al. LRRK2 Pharmacological Inhibition Abates α-Synuclein Induced Neurodegeneration. J Biol Chem. 2015 Jun 15;jbc.M115.660001.
12. Lee BD, Shin J-H, VanKampen J, Petrucelli L, West AB, Ko HS, et al. Inhibitors of leucine-rich repeat kinase-2 protect against models of Parkinson's disease. Nat Med. 2010 Sep;16(9):998–1000.
13. Fell MJ, Mirescu C, Basu K, Cheewatrakoolpong B, DeMong DE, Ellis JM, et al. MLi-2, a Potent, Selective, and Centrally Active Compound for Exploring the Therapeutic Potential and Safety of LRRK2 Kinase Inhibition. J Pharmacol Exp Ther. 2015 Dec;355(3):397–409.
14. Fuji RN, Flagella M, Baca M, Baptista MAS, Brodbeck J, Chan BK, et al. Effect of selective LRRK2 kinase inhibition on nonhuman primate lung. Sci Transl Med. 2015 Feb 4;7(273):273ra15.
15. Andersen MA, Wegener KM, Larsen S, Badolo L, Smith GP, Jeggo R, et al. PFE-360-induced LRRK2 inhibition induces reversible, non-adverse renal changes in rats. Toxicology. 2018 15;395:15–22.
16. Baptista MAS, Merchant K, Barrett T, Bhargava S, Bryce DK, Ellis JM, et al. LRRK2 inhibitors induce reversible changes in nonhuman primate lungs without measurable pulmonary deficits. Sci Transl Med [Internet]. 2020 Apr 22 [cited 2020 Apr 26];12(540). Available from: https://stm.sciencemag.org/content/12/540/eaav0820

17. Tong Y, Yamaguchi H, Giaime E, Boyle S, Kopan R, Kelleher RJ, et al. Loss of leucine-rich repeat kinase 2 causes impairment of protein degradation pathways, accumulation of α-synuclein, and apoptotic cell death in aged mice. Proc Natl Acad Sci. 2010 May 25;107(21):9879–84.
18. Kluss JH, Conti MM, Kaganovich A, Beilina A, Melrose HL, Cookson MR, et al. Detection of endogenous S1292 LRRK2 autophosphorylation in mouse tissue as a readout for kinase activity. Npj Park Dis. 2018 Apr 19;4(1):13.
19. Ritchie ME, Phipson B, Wu D, Hu Y, Law CW, Shi W, et al. limma powers differential expression analyses for RNA-sequencing and microarray studies. Nucleic Acids Res. 2015 Apr 20;43(7):e47–e47.
20. Blighe K, Rana S, Lewis M. EnhancedVolcano: Publication-ready volcano plots with enhanced colouring and labeling [Internet]. Bioconductor version: Release (3.11); 2020 [cited 2020 Jun 2]. Available from: https://bioconductor.org/packages/EnhancedVolcano/
21. Reimand J, Kull M, Peterson H, Hansen J, Vilo J. g:Profiler—a web-based toolset for functional profiling of gene lists from large-scale experiments. Nucleic Acids Res. 2007 Jul;35(Web Server issue):W193–200.
22. Shannon P, Markiel A, Ozier O, Baliga NS, Wang JT, Ramage D, et al. Cytoscape: a software environment for integrated models of biomolecular interaction networks. Genome Res. 2003 Nov;13(11):2498–504.
23. Tomkins JE, Ferrari R, Vavouraki N, Hardy J, Lovering RC, Lewis PA, et al. PINOT: an intuitive resource for integrating protein-protein interactions. Cell Commun Signal. 2020 Jun 11;18(1):92.
24. Lobbestael E, Civiero L, De Wit T, Taymans J-M, Greggio E, Baekelandt V. Pharmacological LRRK2 kinase inhibition induces LRRK2 protein destabilization and proteasomal degradation. Sci Rep [Internet]. 2016 Sep 23 [cited 2020 May 8];6. Available from: https://www.ncbi.nlm.nih.gov/pmc/articles/PMC5034242/
25. Pellegrini L, Hauser DN, Li Y, Mamais A, Beilina A, Kumaran R, et al. Proteomic analysis reveals co-ordinated alterations in protein synthesis and degradation pathways in LRRK2 knockout mice. Hum Mol Genet. 2018 15;27(18):3257–71.
26. Fraser KB, Rawlins AB, Clark RG, Alcalay RN, Standaert DG, Liu N, et al. Ser(P)-1292 LRRK2 in urinary exosomes is elevated in idiopathic Parkinson's disease. Mov Disord. 2016 Oct 1;31(10):1543–50.
27. Wang S, West AB. Caught in the act: LRRK2 in exosomes. Biochem Soc Trans. 2019 Apr 30;47(2):663–70.
28. Lis P, Burel S, Steger M, Mann M, Brown F, Diez F, et al. Development of phospho-specific Rab protein antibodies to monitor in vivo activity of the LRRK2 Parkinson's disease kinase. Biochem J. 2018 Jan 15;475(1):1–22.
29. Purlyte E, Dhekne HS, Sarhan AR, Gomez R, Lis P, Wightman M, et al. Rab29 activation of the Parkinson's disease-associated LRRK2 kinase. EMBO J. 2018 04;37(1):1–18.
30. Sanders LH, Laganière J, Cooper O, Mak SK, Vu BJ, Huang YA, et al. LRRK2 mutations cause mitochondrial DNA damage in iPSC-derived neural cells from Parkinson's disease patients: reversal

by gene correction. Neurobiol Dis. 2014 Feb;62:381–6.

31. Pereira C, Miguel Martins L, Saraiva L. LRRK2, but not pathogenic mutants, protects against H2O2 stress depending on mitochondrial function and endocytosis in a yeast model. Biochim Biophys Acta BBA - Gen Subj. 2014 Jun 1;1840(6):2025–31.
32. Howlett EH, Jensen N, Belmonte F, Zafar F, Hu X, Kluss J, et al. LRRK2 G2019S-induced mitochondrial DNA damage is LRRK2 kinase dependent and inhibition restores mtDNA integrity in Parkinson's disease. Hum Mol Genet. 2017 Nov 15;26(22):4340–51.
33. Mortiboys H, Johansen KK, Aasly JO, Bandmann O. Mitochondrial impairment in patients with Parkinson disease with the G2019S mutation in LRRK2. Neurology. 2010 Nov 30;75(22):2017–20.
34. Mamais A, Chia R, Beilina A, Hauser DN, Hall C, Lewis PA, et al. Arsenite stress down-regulates phosphorylation and 14-3-3 binding of leucine-rich repeat kinase 2 (LRRK2), promoting self-association and cellular redistribution. J Biol Chem. 2014 Aug 1;289(31):21386–400.
35. Denali Therapeutics Announces First Patient Dosed in Phase 1B Study… [Internet]. Denali. [cited 2019 Jan 8]. Available from: https://denalitherapeutics.com/investors/press-release/denali-therapeutics-announces-first-patient-dosed-in-phase-1b-study-of-dnl201-for-parkinsons-disease-1

Figures

Fig. 1

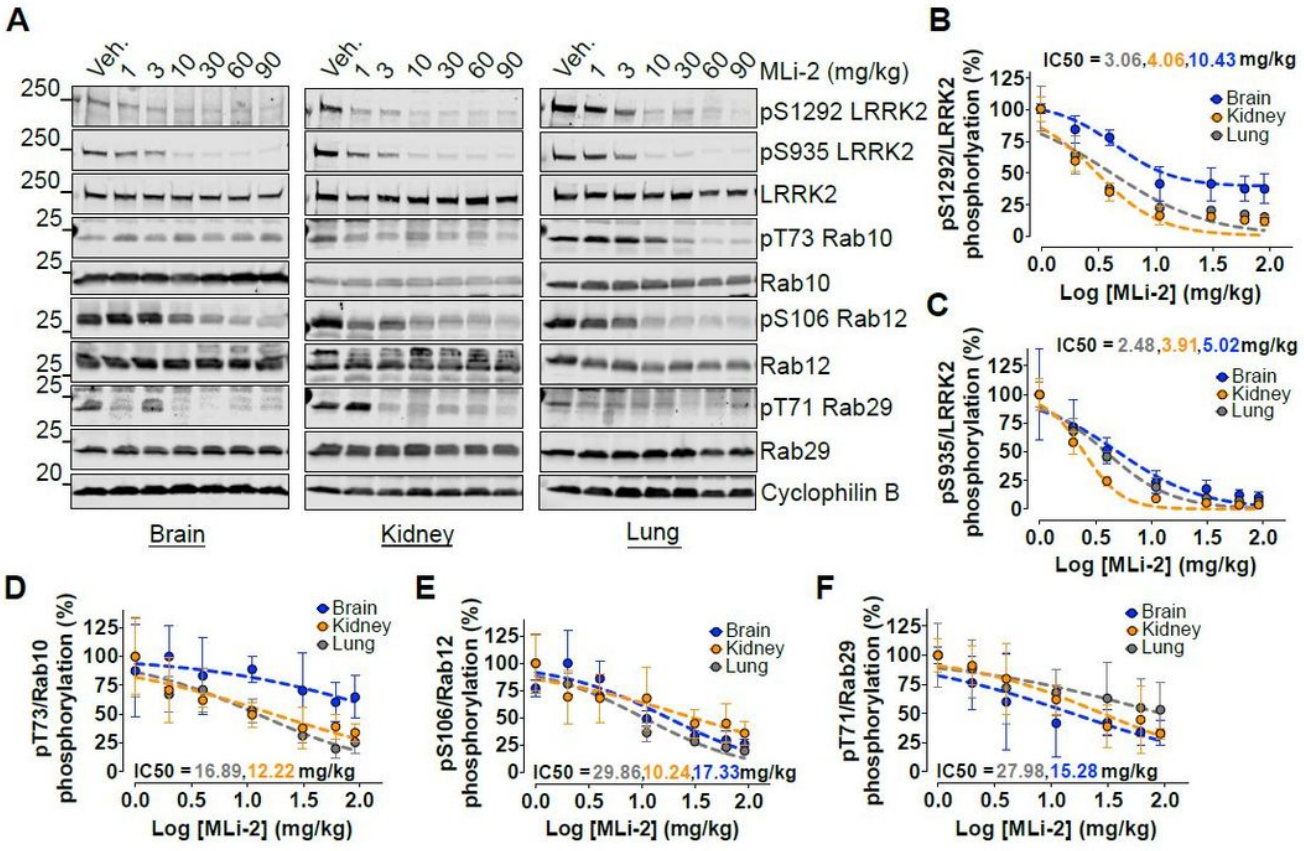

Figure 1

Dose response of acute MLi-2 across brain and peripheral tissues. G2019S LRRK2 knock-in mice were given a single MLi-2 dose via oral gavage and sacrificed 1hr later. Brain, kidney, and lung homogenates were analyzed by western blot (N = 4 per group; 60µg of protein were loaded per well). (A, B, C) Maximal LRRK2 inhibition was achieved at 10mg/kg MLi-2 and plateaued with increasing MLi-2 amounts as seen in S1292 and S935 phosphorylation readouts across all tissues. (D) pT73 Rab10 showed variability in brain but significant dephosphorylation in peripheral tissues with treatment. (E) pS106 Rab12 showed a robust dose-dependent dephosphorylation across all tissues. (F) pT71 Rab29 showed variability but a trend of decrease across all tissues with treatment that reached maximal inhibition at the 30-60mg/kg points. All dose response curves of the phospho-sites are shown in (B-F) and represent percentage over vehicle controls of phospho-levels normalized to total protein levels. IC50 values of Rab GTPases are generally higher and more variable across tissues compared to LRRK2 phosphorylation (IC50s were not reported when 50% reduction was not reached within the dose-response tested).

Fig. 2

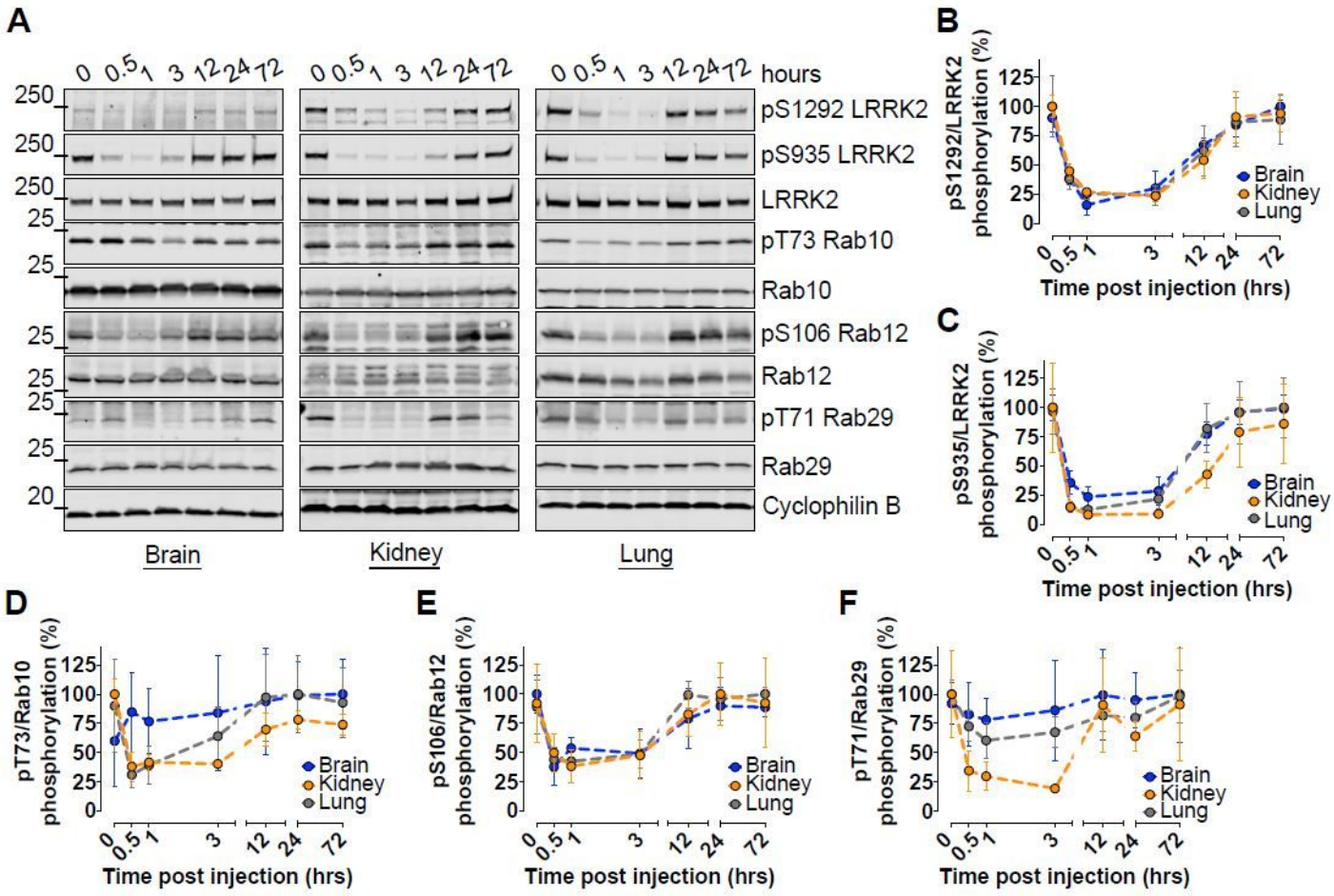

Figure 2

Time-course of target inhibition and rephosphorylation of LRRK2 and Rab GTPase substrates across brain and peripheral tissues. G2019S LRRK2 knock-in mice were given a single 10mg/kg MLi-2 dose via oral gavage and sacrificed at various time points. Brain, kidney, and lung homogenates were analyzed by western blot (n = 4 per group; 60µg of protein were loaded per well) (A). Maximal LRRK2 inhibition was achieved at 1hr post dose as shown by S1292 and S935 dephosphorylation while complete rephosphorylation was achieved by 24hrs (B, C). Rab10 was dephosphorylated by 1hr post-dosing in kidney and lung but not in the brain that showed variability in phosphorylated levels and did not respond to treatment (A, D). Rab12 showed robust dephosphorylation by 1hr in brain and periphery (A, E). Rab29 responded with maximal dephosphorylation in brain and lung by 1hr while kidney showed a slower but more significant response (A, F). All three Rab GTPases recovered their phosphorylation levels by 12hrs post-dose. These results demonstrate that Rab GTPases are dephosphorylated within the first hour following LRRK2 inhibition and rephosphorylate quicker than LRRK2 autophosphorylation recovery following wash-out conditions (~12hrs vs ~24hrs).

Fig. 3

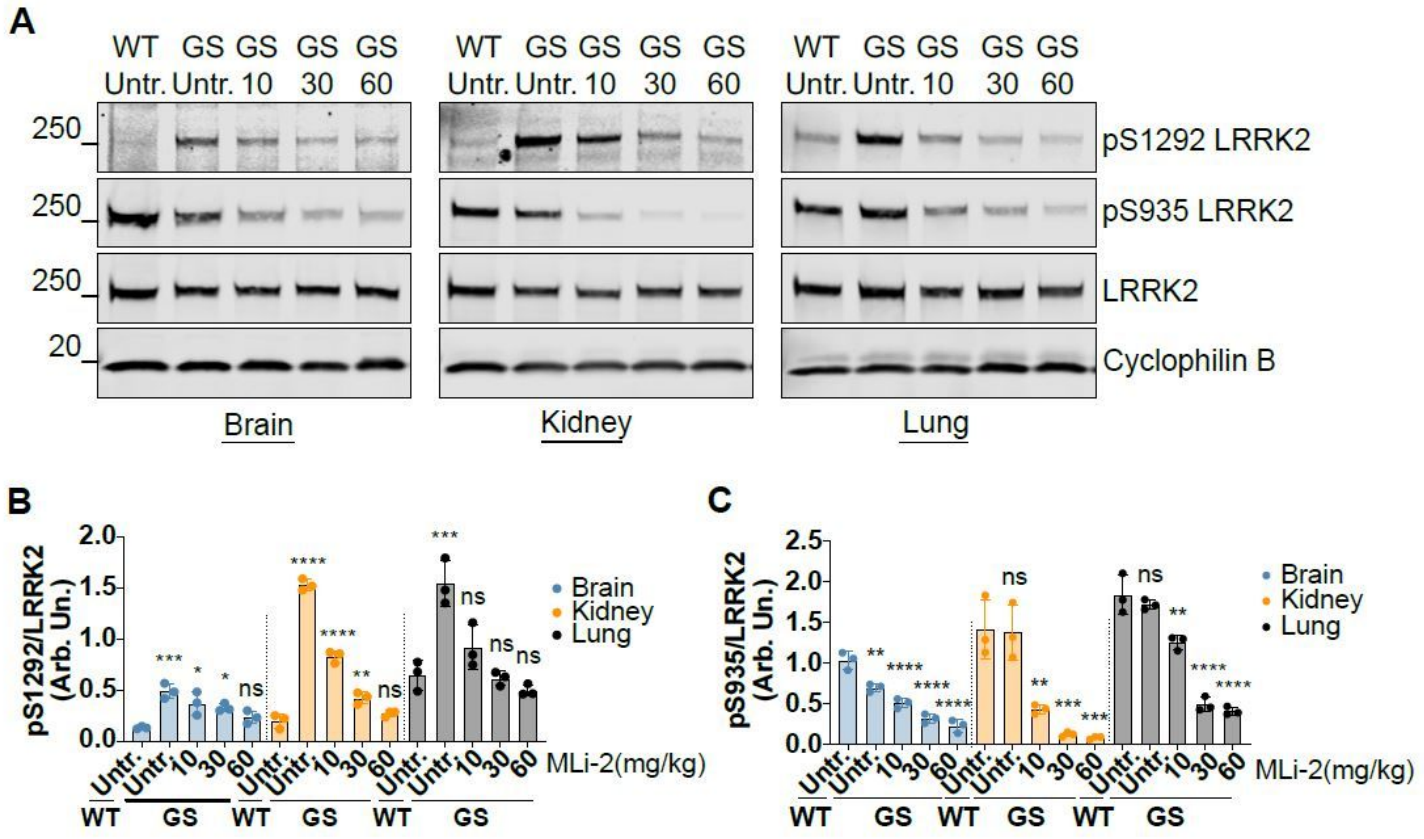

Figure 3

Assessment of MLi-2 in-diet dosing and LRRK2 inhibition. G2019S LRRK2 knock-in mice were fed chow containing different concentrations of MLi-2 to reach 10, 30, or 60mg/kg/day dosing compared to G2019S knock-in and WT LRRK2 cohorts that were fed control chow. After 10-days, animals were

sacrificed 2-3 hrs post start of their light cycle. Western blots of brain, kidney and lung tissue samples are shown. (A, B) Across all tissues, a significant increase in S1292 phosphorylation is seen in G2019S mice compared to WT animals which is ameliorated with increasing MLi-2 doses reaching WT levels at 60mg/kg/day. (C) A dose-response was seen in S935 dephosphorylation that plateaued at 30mg/kg/day. Quantitation of phosphorylation levels is calculated as S1292 and S935 levels over total LRRK2 (B and C: one-way ANOVA with Tukey's post hoc, ****P < 0.0001, ***P < 0.0002, **P < 0.0021, *P <0.0332; N = 3; SD bars shown; (B) F(14, 30) = 52.27, (C) F(14, 30) = 56.58).

Fig. 4

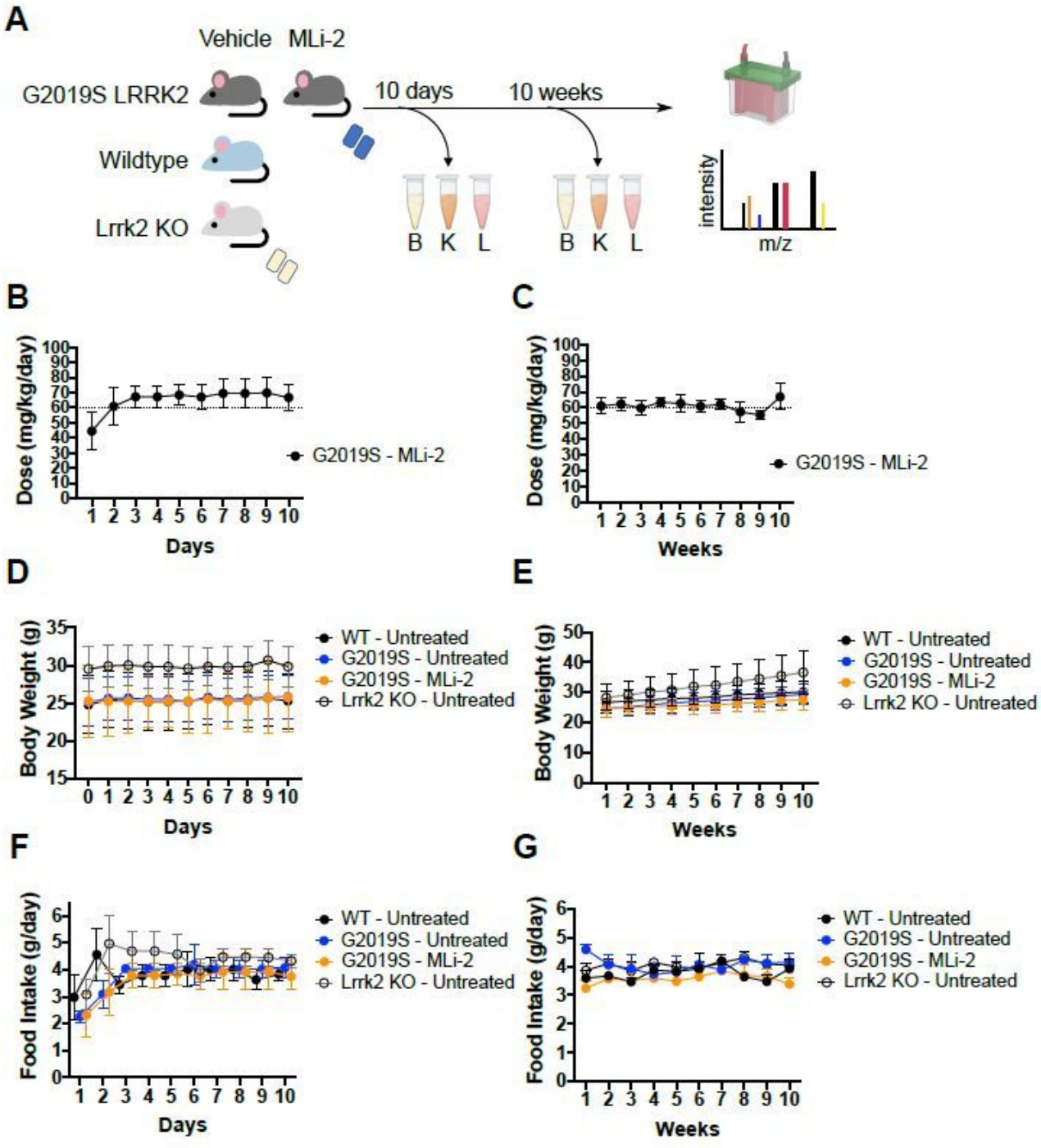

Figure 4

Experimental design and dosing paradigm of the chronic in vivo MLi-2 proteomics experiment. (A) Schematic of experimental design for the chronic MLi-2 proteomics experiment. (B) 10-Day cohort animals observed no weight changes and consumed ~4g of chow per day (C). Daily dose of MLi-2 was calculated by body weight and food intake and showed that animals on average received ~65mg/kg/day of drug (D). (E) 10-Week cohort animals grew 3-8g in body weight over the course of 10 weeks, with an average food intake of 4g (F) and hit the 60mg/kg/day mark each week (G).

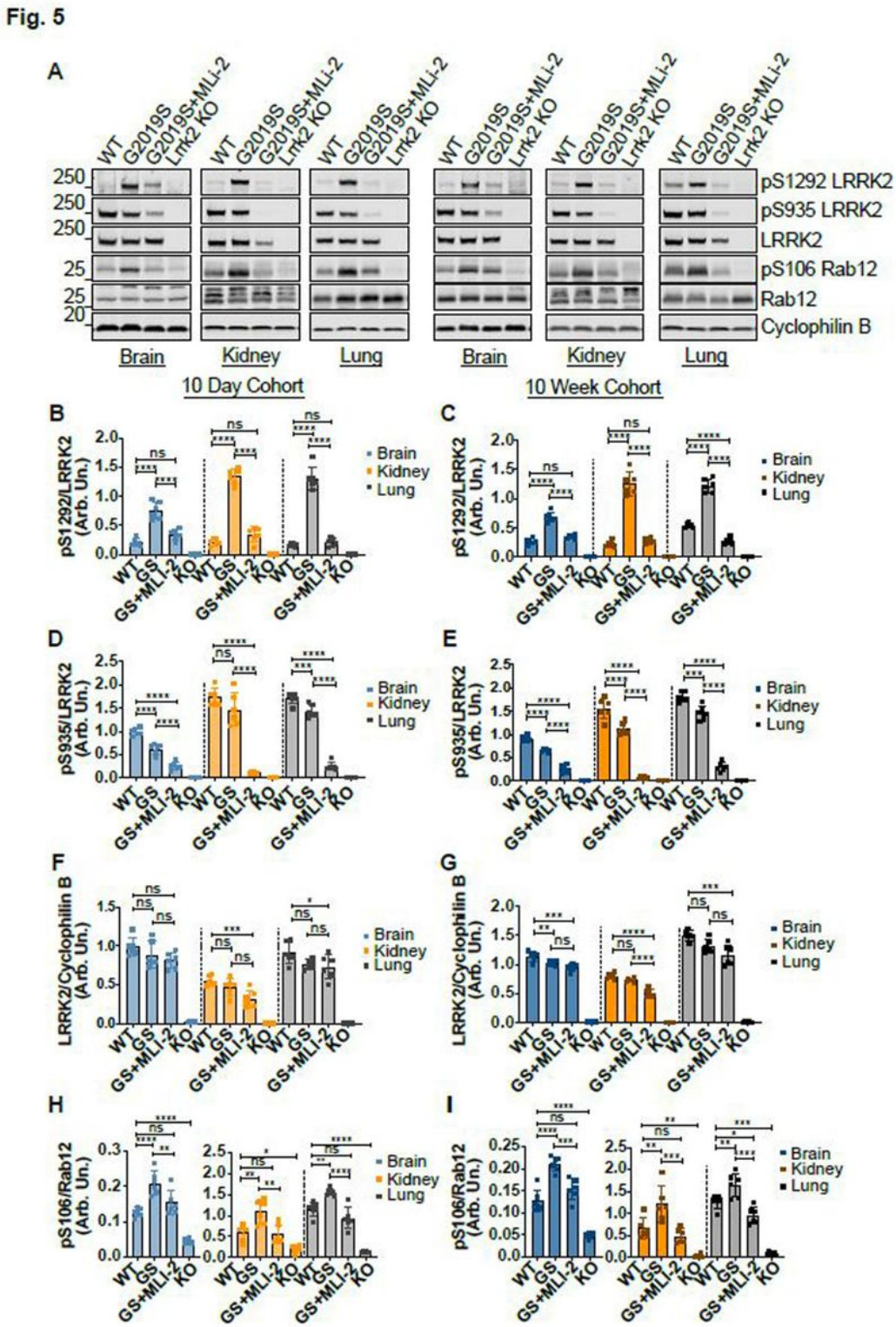

Figure 5

LRRK2 and S106 Rab12 phosphorylation following chronic MLi-2 treatment. WT, G2019S LRRK2 KI, and LRRK2 KO mice were fed vehicle or MLi-2-containing chow over the course of 10 days or 10 weeks (A). LRRK2 inhibition is maintained between the short-term (10-day) and long-term (10-week) chronic treatment as shown by decrease in pS1292 (B, C) and pS935 levels (D, E) to levels comparable to WT controls. A decrease in total LRRK2 levels is observed in peripheral tissues with chronic treatment in by 10 days (F) and is exacerbated in the 10-week treatment (G). S106 Rab12 phosphorylation levels show a significant decrease with treatment to levels comparable to WT tissue (H, I). One-way ANOVA with Tukey's post hoc; N = 6; ****P <0.0001, ***P <0.0002, **P <0.005, *P <0.05; (B) $F(11, 60)= 146.8$, (C) $F(11, 60)= 178.7$, (D) $F(11, 60)= 158.0$, (E) $F(11, 60)= 265.9$, (F) $F(11, 60)= 75.97$, (G) $F(11, 60)= 271.5$, (H) $F=(11, 60)= 65.78$, (I) $F(11, 60)= 59.67$.

Fig. 6

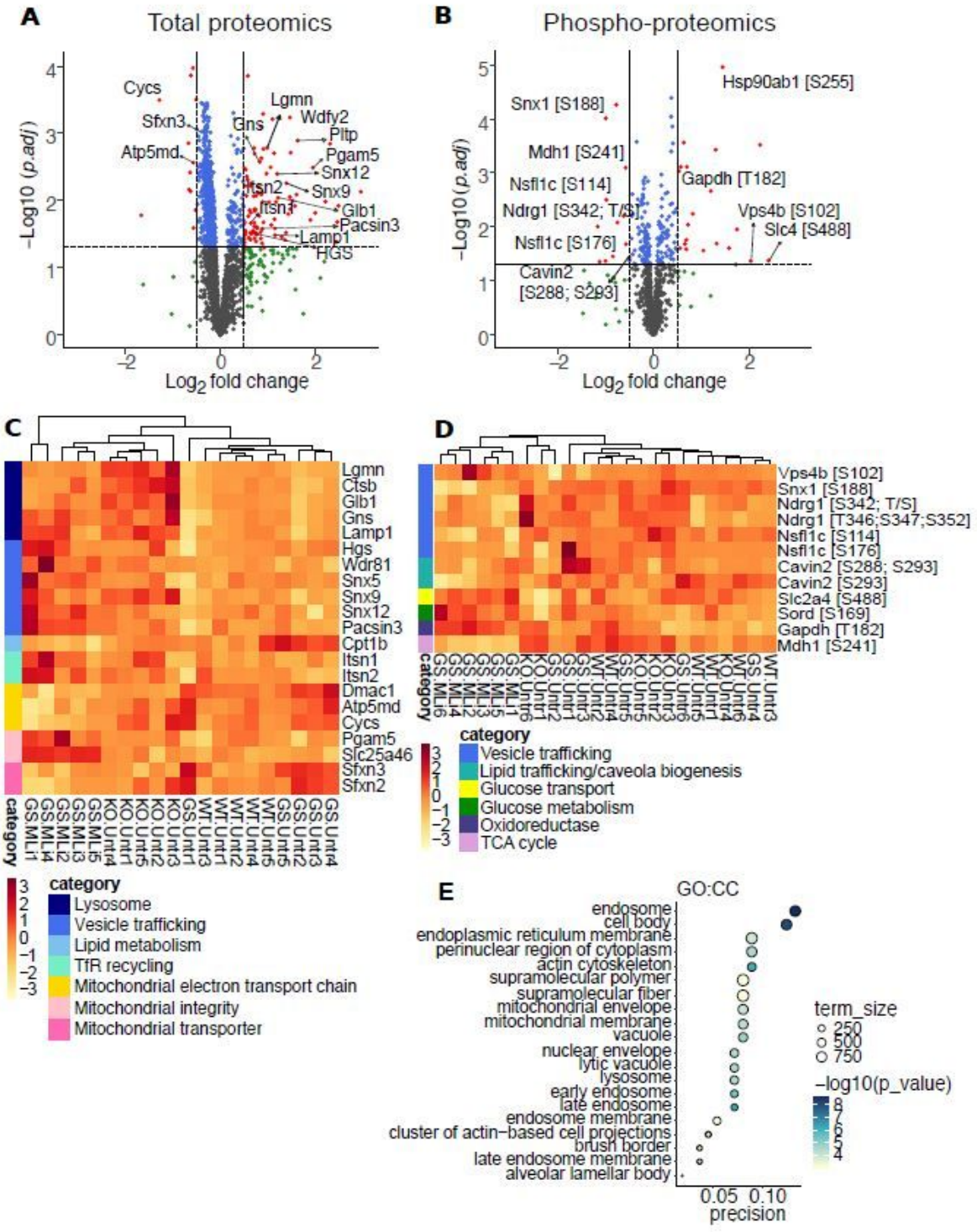

Figure 6

Proteomic analysis of changes in kidney between G2019S LRRK2 MLi-2 and G2019S vehicle 10-week treated mouse cohorts. Volcano plot showing changes in protein levels following chronic treatment, depicted as log2 fold changes (x-axis) versus the −log10 of adjusted P-values (y-axis) for each protein (A). A number of endolysosomal proteins were upregulated, including legumain and other lysosomal proteases in kidneys of G2019S LRRK2 KI mice that received chronic MLi-2 treatment for 10 weeks,

compared to vehicle G2019S KI controls. Heat maps of selected significant hits across the WT, G2019S KI and LRRK2 KO vehicle cohorts as well as the G2019S KI chronic MLi-2 cohort, highlighting proteins involved in vesicular trafficking, lipid metabolism, transferrin recycling and mitochondrial homeostasis. Using unsupervised hierarchical clustering we show that the G2019S MLi-2 and LRRK2 KO mice cluster together, suggesting that chronic LRRK2 inhibition mimics a LRRK2 KO effect in kidney (B). Volcano plot showing changes in phospho-proteins in G2019S MLi-2 treated vs G2019S untreated mice, highlighting dysregulation of proteins involved in trafficking, glucose transport and metabolism, and the TCA cycle (C, D). Bubble plot showing GO:CC term enrichment in the significant phospho- and total kidney proteomics hits highlights enrichment for endolysosomal processes (E). Volcano plots key: grey = non-significant, blue = <0.05 P-value, green = >1.4x log fold change, red = <0.05 P-value and >1.4x log fold change.

Fig. 7

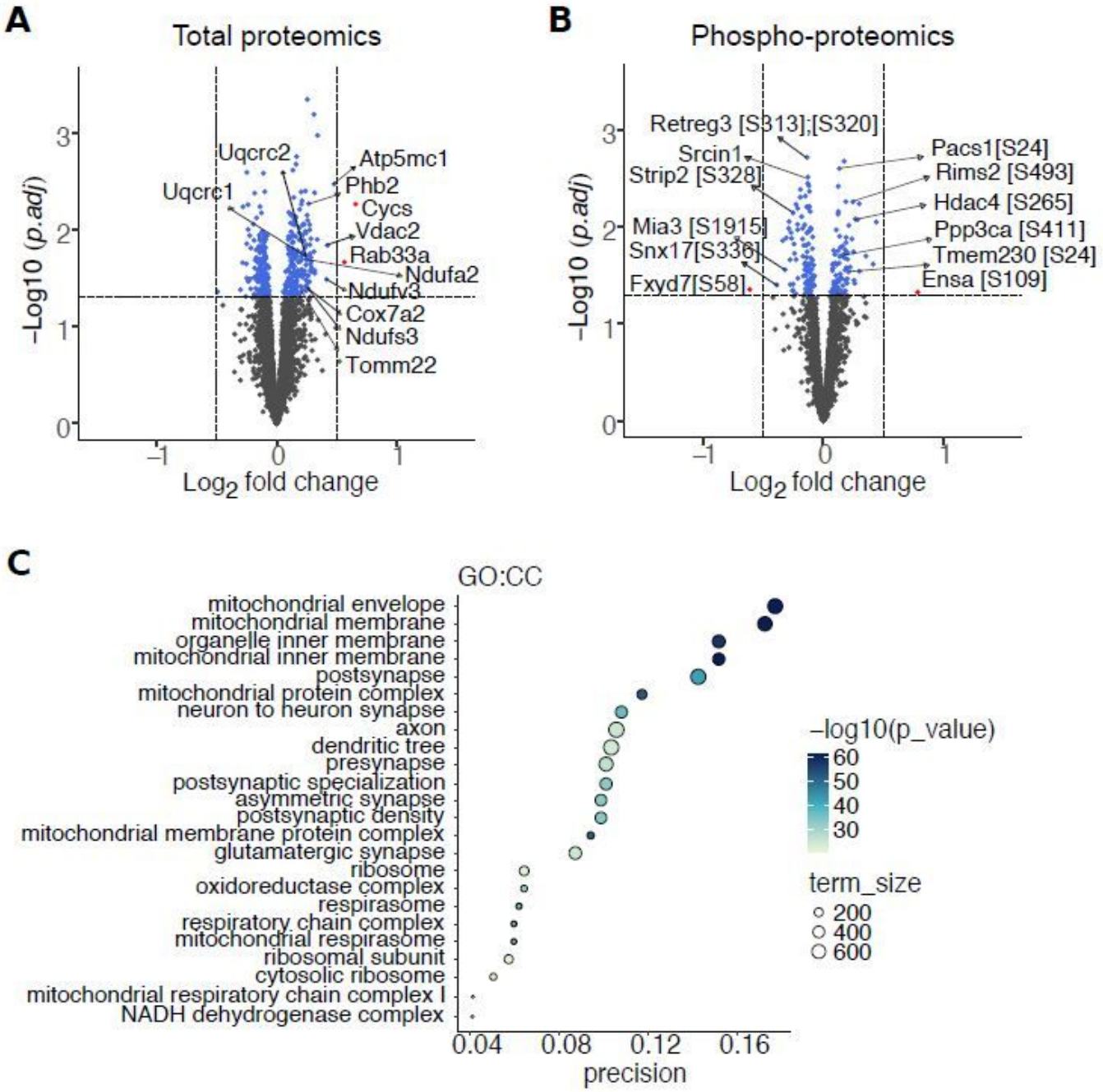

Figure 7

Proteomic analysis of changes in brain between G2019S LRRK2 MLi-2 and G2019S vehicle 10-week treated mouse cohorts. A volcano plot from total proteomics of whole brain tissue comparing the G2019S chronic MLi-2 cohort versus G2019S KI vehicle controls. Modest upregulation was observed in mitochondrial proteins with treatment, specifically proteins of the electron transport chain (A). Changes in phosphopeptides with treatment highlighted proteins involved in vesicular trafficking and postsynaptic

regulation (B). GO:CC term enrichment bubble plot was generated from the significant hits of the total and phospho-proteomics showing high enrichment for mitochondrial compartments, as well as proteins associated with postsynaptic function (C). Volcano plots key: grey = non-significant, blue = <0.05 P-value, green = >1.4x log fold change, red = <0.05 P-value and >1.4x log fold change.

Fig. 8

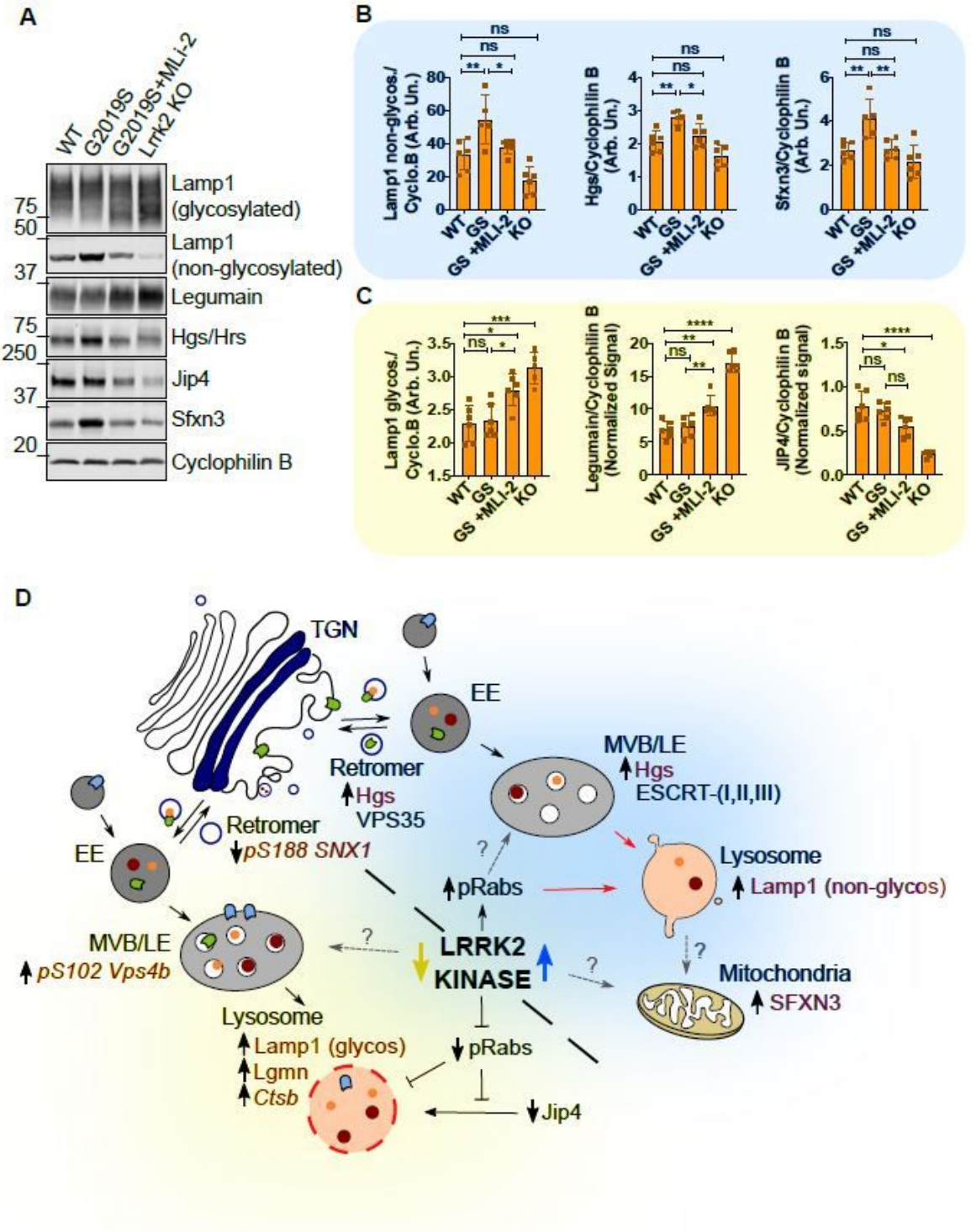

Figure 8

Validation of proteomic hits reveal both rescue of mutant-driven effects and dysregulatory patterns in long-term MLi-2 treated mice. Follow-up validation of proteomics hits in Western blot confirmed differential changes to endolysosomal, trafficking, and mitochondrial proteins. Within these proteins, we observed divergent patterns of therapeutic and dysregulatory effects in the kidneys of 10-week, MLi-2 treated G2019S KI mice (A). Therapeutic trends were observed in non-glycosylated Lamp1, Hgs, and Sfxn3, in which high expression of these proteins in untreated G2019S KI mice were ameliorated down to wildtype levels with LRRK2 inhibition (B). We also observed significant increases in glycosylated Lamp1 and Legumain towards levels observed and previously characterized in Lrrk2 KO mice. Additionally, we have shown a significant decrease in Jip4 within the treated mice that were also exacerbated in Lrrk2 KO mice (C). Based on these discoveries, we have hypothesized divergent mechanisms for LRRK2 hyperactivity and chronic inhibition (D). The proteins in maroon reflect the proteins identified in our proteomics screens (italicized) and validation on WB (not italicized). The grey dashed arrows depict unknown mechanism/relationship with LRRK2 kinase activity. One-way ANOVA with Tukey's post hoc; N = 6; ****P <0.0001, **P <0.005, *P <0.05; (B) non-glycosylated Lamp1: $F(3, 19)= 13.58$, Hgs: $F(3, 19)= 13.72$, Sfxn3: $F(3, 19)= 9.323$, (C) glycosylated Lamp1: $F(3, 19)= 13.70$, Legumain: $F(3, 20)= 61.36$, Jip4: $F(3, 20)= 27.39$.

Supplementary Files

This is a list of supplementary files associated with this preprint. Click to download.

- supplement5.xlsx
- supplement6.pdf